Available online at www.sciencedirect.com
SCIENCE DIRECT®
PERGAMON
International Journal of Multiphase Flow 29 (2003) 1395–1412
International Journal of Multiphase Flow
www.elsevier.com/locate/ijmulflow

Incipient flooding in inclined tubes of small diameter

A.A. Mouza, S.V. Paras, A.J. Karabelas *

Department of Chemical Engineering and Chemical Process Engineering Research Institute, Aristotle University of Thessaloniki, Univ. Box 455, GR 54124, Thessaloniki, Greece

Received 23 April 2002; received in revised form 10 June 2003

Abstract

This is an experimental study on the effect of tube diameter, inclination angle and liquid properties on incipient flooding in inclined small diameter tubes, in gas–liquid counter-current flow. Flooding experiments are conducted with four relatively small i.d. tubes (6, 7, 8 and 9 mm) in the range of inclination angles 30–60° and smooth inlet/outlet, i.e. a porous tube segment for the liquid and tapered section for gas entry. The effect of liquid properties is examined by using two different liquids, namely water and kerosene. To facilitate the interpretation of flooding data, the free-flowing liquid layer characteristics are also investigated. The results indicate that under these conditions, the effect of tube i.d. and angle of inclination on incipient flooding is significant, but the influence of liquid physical properties is most pronounced.

Keywords: Flooding; Counter-current flow; Inclination; Small diameter tube

1. Introduction

In recent years there is considerable interest in counter-current gas/liquid flow through narrow passages, mainly in connection with the development of compact heat and/or mass transfer devices. *Flooding phenomena* for counter-current flow *in inclined small diameter tubes* have attracted attention because of the limitations they pose in the operation of novel reflux condensers or other types of heat exchange equipment (e.g. Celata et al., 1992). This work is part of a study aimed at improving our physical understanding and modeling the operation of compact reflux type

* Corresponding author. Tel.: +30-2310-996201; fax: +30-2310-996209.
E-mail address: karabaj@cperi.certh.gr (A.J. Karabelas).

0301-9322/$ - see front matter
doi:10.1016/S0301-9322(03)00124-1

contactors made of corrugated plates. Corrugations are arranged at an angle, with respect to the vertical, which appears to play a significant role in flow pattern development, including incipient flooding. Typical angles of such inclination are 30–60°, whereas the flow passages created by corrugations (furrows) are characterized by equivalent diameters of order 10 mm. Liquid loadings of interest are small to moderate corresponding to superficial liquid Reynolds numbers $Re_{LS} = U_{LS}D/v$ in the range 10–10^3. In a companion paper (Mouza et al., 2002), incipient flooding was studied, under the above conditions, for *vertical* small diameter tubes. In the present paper, the effect of inclination angle is investigated within the aforementioned range of conditions.

Although a great deal of work has been carried out in the past few decades, there is still considerable uncertainty concerning the mechanisms causing flooding as well as the most appropriate correlations for practical applications. Review papers (e.g. Bankoff and Lee, 1986; Hewitt, 1995) provide a good account of this research, which deals mainly with experiments in *vertical* tubes with i.d. much larger than the sizes considered here. To the best of authors' knowledge, flooding in inclined *small diameter* tubes has received inadequate attention. Most of the reported flooding data have been obtained in inclined tubes with diameters greater than 20 mm. Hewitt (1977) reported data on flooding in vertical and inclined tubes of 32 mm i.d., and pointed out the significance of entry conditions. Barnea et al. (1986) studied air–water counter-current flow in a 51 mm i.d. tube for a wide range of inclination angles (1–90° from horizontal). Celata et al. (1992) conducted their experiments in 20 mm i.d. tubes and for steep inclinations (75–90° from horizontal). Zapke and Kroeger (1996) investigated flooding mainly in a vertical 30 mm i.d. tube for various liquids and gases; only limited data were reported at an inclination angle 60° with respect to horizontal. Wongwises (1998) studied flooding in a 29 mm tube for various inclination angles (60–85°); his reported gas velocities for incipient flooding are much lower than those predicted by the other investigators.

In general, the factors that tend to influence the onset of flooding (e.g. Hewitt, 1995; Zapke and Kroeger, 1996) are the conduit dimensions, the type of liquid and gas entry, the liquid properties and the inclination angle. Due to this multitude of factors and the complexity of the mechanisms involved, reliable predictive tools of general validity are not available at present, even for flooding in relatively large diameter tubes for which data are available. In their effort to elucidate the complicated effect of inclination angle on flooding in counter-current stratified flow Barnea et al. (1986) point out some (intuitively) counter acting trends *with increasing angle* of inclination; i.e. the decreasing thickness of faster flowing liquid layer, the increasing height of waves at the gas/liquid interface, and the increasing tendency for lateral wave spreading. They report, as a net effect, that the critical flooding velocity tends to "...increase and then decrease as the inclination angle is changed from horizontal to vertical...".

The most widely used correlation for the flooding limit (although quite often unsuccessfully, Bankoff and Lee, 1986) is due to Wallis (1969), which was developed for *vertical* tubes and does not take into consideration the effect of fluid properties (i.e. viscosity, surface tension). In order to include the tube inclination and gas inlet configuration on flooding, Zapke and Kroeger (1996) employ a modified version of the Wallis expression, where the effect of the fluid properties is also incorporated, as follows:

$$\sqrt{U_G^*} + m\sqrt{U_L^*} = EZ_L^b \tag{1}$$

where

$$U^*_{G,L} = U_{GS,LS}\sqrt{\frac{\rho_{G,L}}{gD(\rho_L - \rho_G)}} \tag{2}$$

is a dimensionless velocity with U_{GS} and U_{LS} the superficial gas and liquid velocities, respectively.

$$Z_L = \frac{\sqrt{D\rho_L\sigma}}{\mu_L} \tag{3}$$

is the inverse Ohnesorge number, where ρ_L, μ_L, σ are properties of the liquid phase. b, E and m designate empirical constants that depend on tube inclination angle and tube-end configuration.

The above expression (Eq. (1)), which implies that there is a linear relationship between $\sqrt{U^*_L}$ and $\sqrt{U^*_G}$, was tested for various liquids with a fairly broad range of viscosity ($0.57–2.5 \times 10^{-3}$ kg/m s) and surface tension ($23–72 \times 10^{-3}$ N/m). However, as the experiments were conducted with only one i.d. tube, its validity for other (especially smaller) diameters is still untested.

The scope of this work is to improve our understanding of the effect of tube diameter, inclination angle and fluid properties on the mechanisms triggering incipient flooding in small diameter tubes. Flooding experiments are reported herein with four different tube inside diameters, namely 6, 7, 8 and 9 mm, with smooth inlet and outlet conditions for air and liquid, in the range of inclination angles 30–60° with respect to horizontal. In an attempt to examine the effect of the liquid properties on flooding two different liquids, namely water and kerosene, are used. To facilitate the interpretation of flooding data, the free-flowing liquid layer characteristics are also investigated.

2. Experimental set-up and procedures

Fig. 1 shows the experimental set-up employed for the counter-current flow tests with various tube diameters (i.d. = 6, 7, 8 and 9 mm) and inclination angles (30–60° from horizontal position). The test tubes (60 cm long) were made of glass. Two liquids were used, namely water and kerosene, and their physical properties are given in Table 1. The wetability of the glass tube was improved by treating its inner surface before each set of experiments with a *silica sol*. The experiments were conducted at ambient temperature and pressure conditions. Care was taken to minimize disturbances introduced at air and liquid inlet. Air enters at the bottom, through a small tube (i.d. = 6 mm) placed concentrically with the test tube, which is tapered at the end, whereas the liquid phase is introduced uniformly at the top through a specially machined porous wall segment. The work of Govan et al. (1991), carried out in *vertical* tubes, suggests that the design employed in this study may offer the smoothest possible gas entry and quite reproducible data for inclined tubes. The removal of the liquid through a porous wall segment above the gas entry (which might also create smooth entry conditions) is not feasible for the large inclination angles employed here. A more detailed description of the experimental set-up is given elsewhere (Mouza et al., 2002).

In an effort to gain insight into the basic mechanisms triggering flooding, direct visual observations were made as well as recordings using a *Redlake MotionScope PCI*® high-speed camera to capture details of the flow. Pictures were taken at a speed of 250 frames/s and a shutter rate of 1/1000, over a fairly broad range of flow rates and at three different locations along the pipe,

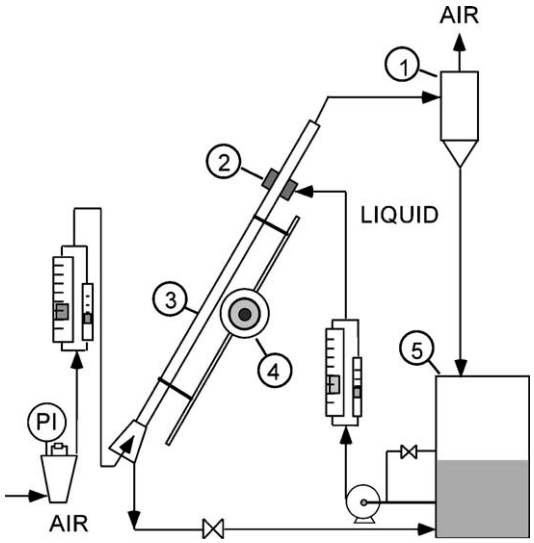

Fig. 1. Experimental flow loop: (1) phase separator; (2) porous wall section; (3) glass test tube; (4) rotating support; (5) liquid storage tank.

Table 1
Physical properties of fluids

	Kerosene	Water	Air
Density, ρ (kg/m^3)	800	1000	1.2
Viscosity, μ (kg/m s)	1.4×10^{-3}	1.0×10^{-3}	1.8×10^{-5}
Surface tension, σ (kg/s^2)	0.028	0.072	–

i.e. just below the liquid entrance, at the liquid exit, and at an intermediate location. Details concerning the visualization method can be found in a recent paper by Mouza et al. (2002). The results from several such experimental runs, conducted with *four* tube diameters for various inclination angles and over a range of *water* and *kerosene* flow rates, are presented in a subsequent section.

An attempt was made to obtain experimentally the mean free-flowing layer thickness in the absence of airflow. Hence a series of experiments without counter-current gas flow was conducted and the recorded images were used to extract both *qualitative* and *quantitative* information on free-flowing layers. With proper lighting the free cross-section of the tube and the flowing layer thickness are clearly identified in the pictures as shown in Fig. 2. Using appropriate software the liquid film trace can be obtained at a specific point along the tube. The calibration of the measuring system is accomplished by determining from the pictures both the inner (i.d.) and outer (o.d.) diameter of the tube (Fig. 2a and c), which are also obtained by accurate direct measurements. It is pointed out here that, as is evident from Fig. 2, the refractive index of the liquids employed is rather close to that of the glass, and quite different from that of air. Therefore, with the optical system used, only two interfaces can be discerned; i.e. the (fixed) outer air/tube interface and the (varying) inner liquid/air one. This is shown in Fig. 2 where one can distinguish the

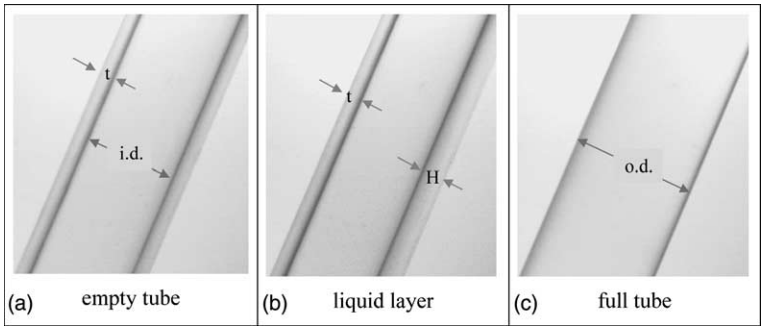

Fig. 2. Photos of the tube showing the characteristic quantities measured by the optical method. i.d./o.d. = tube inside/outside diameter; t = wall thickness; H = wall thickness + flowing layer thickness.

tube i.d. and o.d. as well as the tube thickness, t. The actual liquid film thickness, h, is obtained by subtracting the known wall thickness, t, from the measured "total thickness", H. The film thickness measurements reported here are taken at $L \approx 60$ cm from the top (i.e. above the liquid exit), a distance considered to be beyond the initial liquid layer development length for the liquid Reynolds numbers examined (e.g. Pierson and Whitaker, 1977).

3. Flooding in inclined small diameter tubes

3.1. Critical flooding velocities

It is generally accepted that flooding is characterized by a sustained liquid flow above the liquid inlet, accompanied by a sharp rise of the pressure drop in the test section (Bankoff and Lee, 1986). The critical gas velocity at the *onset* of flooding reported here, is associated with the first appearance of liquid flow reversal.

In Figs. 3 and 4 the superficial gas Reynolds number, $Re_{GS} = U_{GS}D/v_G$, is plotted versus the corresponding superficial liquid Reynolds number $Re_{LS} = U_{LS}D/v_L$ for a range of inclination angles, where U_{GS} and U_{LS} are the superficial gas and liquid velocities at the onset of flooding and D the tube inside diameter. The effect of tube diameter on the form of flooding curve is presented in Fig. 4, whereas the effect of fluid type is shown in Fig. 3. Designations of experimental data sets, plotted in these figures, are summarized in Table 2.

Three distinct regions are generally observed in the above curves (Fig. 3a), which are more pronounced in the small diameter tubes. In *Region A*, which corresponds to the lower liquid flow rates, the gas Reynolds number and hence the superficial gas velocity, U_{GS}, at the onset of flooding tends to increase with the liquid Reynolds number. The extent of Region A seems to depend on the tube diameter and tends to disappear for the larger tube i.d. employed here (Fig. 3b). This is probably why the existence of this region has not been reported so far in the literature, where experiments with larger diameter tubes (e.g. i.d. = 26 or 50 mm) are usually presented. It will be noted that the slope of the flooding curve depends on the liquid properties (Fig. 3a and b). For example, the present experiments reveal that with kerosene the slope of the flooding curve in

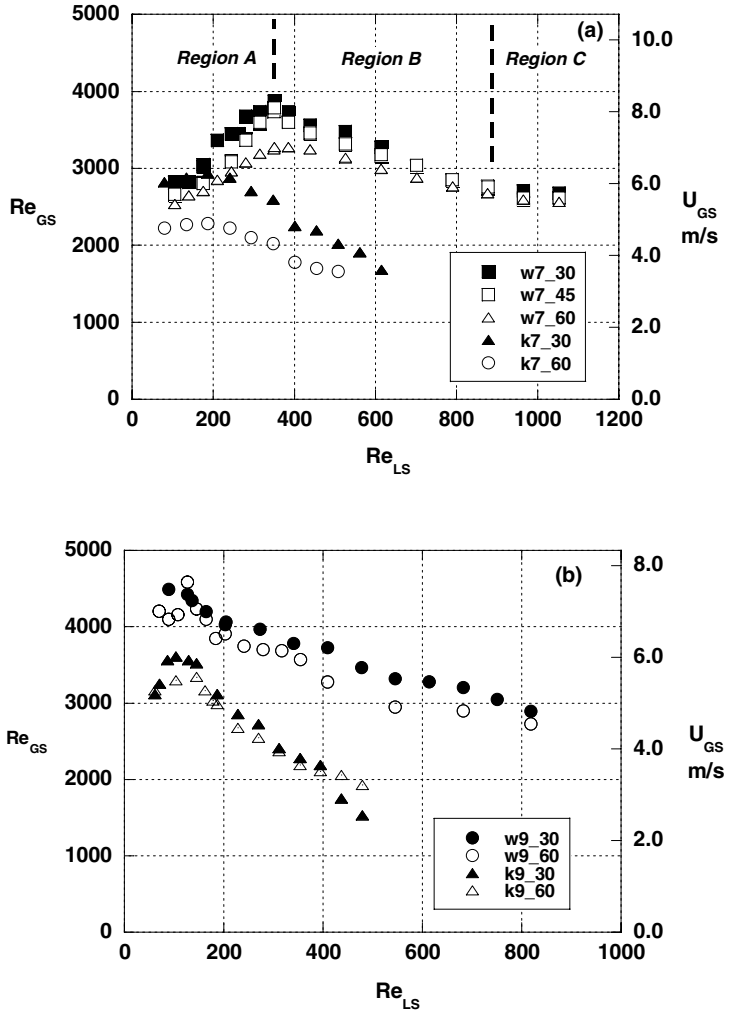

Fig. 3. The gas Reynolds number at incipient flooding versus the corresponding liquid Reynolds number, showing the effect of fluid type on the form of flooding curve. Data at $\varphi = 30°$, 45° and 60°. (a) i.d. = 7 mm; (b) i.d. = 9 mm.

Region A is very small, i.e. the gas flooding velocity is almost constant; however, for water under the same conditions this slope is much greater (Fig. 3a).

In *Region B* the gas velocity required for incipient flooding tends to decrease with increasing liquid Reynolds number. This trend is usually reported in the literature for tests with relatively large tube diameters. It appears that the extent of this region and the slope of the curve depend on tube diameter (Fig. 4) as well as on type of fluid (Fig. 3).

Finally, in *Region C* flooding appears to be initiated at a gas Reynolds number which is weakly dependent on liquid flow rate and tends to a constant value at high Re_{LS}. Visual observations described in the next section, reveal that Region C corresponds to a different mechanism triggering flooding compared to that for Regions A and B. The liquid Reynolds number, which marks

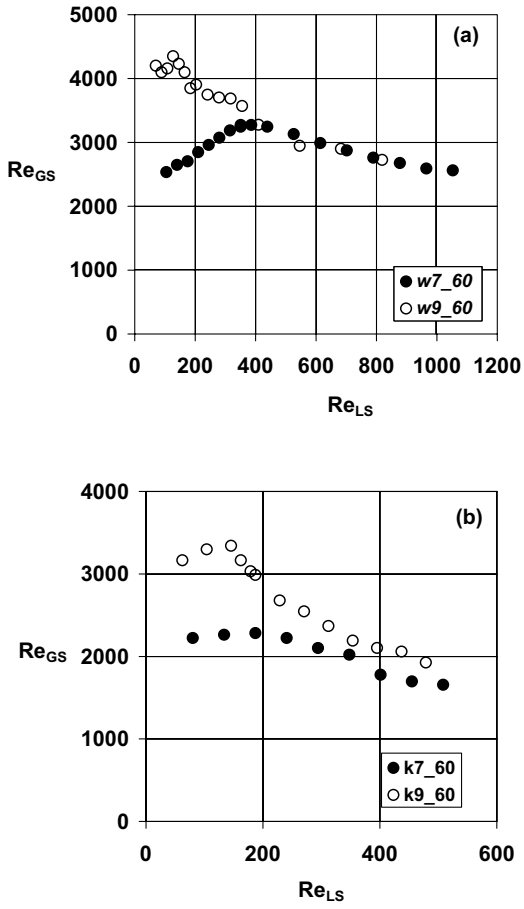

Fig. 4. The superficial gas Reynolds at incipient flooding number versus the corresponding liquid Reynolds number, showing the effect of tube diameter on the form of flooding curve: (a) water; (b) kerosene.

the beginning of Region C, depends on the parameters that determine the extent of the previous Region B. Thus, for the flow rates examined in the present study Region C is not observed when kerosene is used (Fig. 3). The value of the nearly constant gas Reynolds number in Region C (for water) does not seem to depend on the inclination angle (Fig. 3a) but may depend on tube diameter.

3.2. Visual observations on flooding

The visual observations reveal that in the inclined tube (30–60° from horizontal) a stratified counter-current flow is established, where the liquid surface appears to be smooth and undisturbed at low gas velocities. As the gas velocity increases small amplitude waves begin to form on the liquid surface. The liquid flow is driven by the gravity forces parallel to the direction of flow and opposed by the interfacial shear (τ_i) generated by the rather high gas velocity as well as the

Table 2
Designation of experimental runs

Run	Liquid	Tube i.d., mm	Inclination, deg
*w*6_30	Water	6	30
*w*7_30		7	30
*w*7_45		7	45
*w*7_60		7	60
*w*8_30		8	30
*w*9_30		9	30
*w*9_60		9	60
*k*7_30	Kerosene	7	30
*k*7_60		7	60
*k*9_30		9	30
*k*9_60		9	60

wall shear stress (τ_w). Surface tension forces and the gravity force component perpendicular to the direction of flow exert a stabilizing effect on the waves.

Region A: As already mentioned, in the absence of airflow the liquid surface appears quite smooth and undisturbed. The visual observations and the video recordings reveal that in Region A and at relatively low gas velocities long-wavelength and small-amplitude waves begin to form on the liquid surface. An increase of the gas velocity causes further wave growth. As gas velocity approaches incipient flooding, the motion of a wave appears to be momentarily arrested near the liquid exit, with a tendency to grow by the accumulation of liquid falling along the tube wall. At this point, a slight increase of the gas flow rate appears to initiate reversal of the wave motion and to cause the liquid from the wave crest at the tube bottom to spread in the circumferential direction leading to fairly coherent "ring"-type waves, especially in the small i.d. tubes (Fig. 5a). The upward transport of these "ring"-type waves is considered as the onset of flooding.

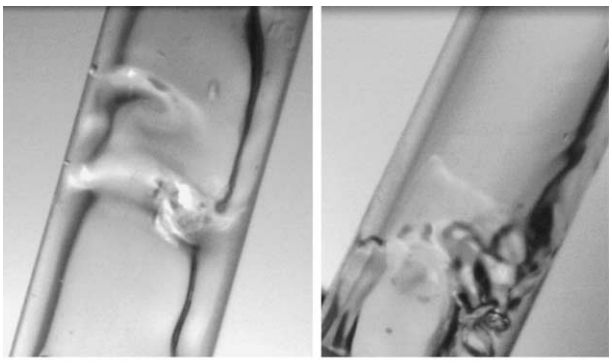

Fig. 5. Effect of tube diameter on the type of ascending waves in Region A: (a) i.d. = 7 mm, $Re_{LS} = 80$ and (b) i.d. = 9 mm, $Re_{LS} = 62$.

The existence of Region A is pronounced in the smaller diameter tubes, where the formation of "ring"-type waves (through wave spreading) is apparently easier (Fig. 5a). In the case of kerosene, its lower surface tension facilitates both the formation of waves and the lateral liquid spreading. Consequently, for the same liquid Reynolds number, the gas Reynolds number required for incipient flooding is smaller if kerosene is used (Fig. 3). With increasing liquid flow rate, the observed gas velocity for incipient flooding tends to increase.

In the 9 mm i.d. tube the extent of Region A is reduced for the case of kerosene and almost disappears for the case of water (Fig. 3b). As already mentioned, in the smaller i.d. tubes tested here (i.e. i.d. = 6 and 7 mm) "ring" type (annular) waves were observed to form quite readily, almost independently of inclination angle. In such small diameter tubes the greater curvature may facilitate lateral liquid spreading and the development of rather symmetric "ring-type" waves. For the larger diameter tubes (8 and 9 mm i.d.) growth of standing waves at the liquid exit and reversal of their motion is again observed. Lateral spreading of liquid at the onset of flooding appears to take place but the upward moving waves are rather asymmetric with more liquid at the tube bottom. The picture in Fig. 5b shows such an asymmetric, upward moving wave at very low kerosene superficial velocity ($U_{LS} = 0.012$ m/s). Some liquid droplets torn off the wave crest are observed in the gas core traveling upwards.

Region B: In this region the gas flooding velocity tends to decrease with increasing liquid superficial velocity. The data roughly follow a Wallis type correlation and the trend is in agreement with previous works reported in the literature (e.g. Zapke and Kroeger, 1996). Kerosene and water flooding curves have almost the same slope, but the gas velocity required to initiate flooding is always *greater* when water is used (Fig. 3). In this region, flooding is also initiated at the liquid exit by the growth and the upward transport of the waves formed on the liquid layer at the tube bottom. At the onset of flooding, the waves reverse their flow direction, while spreading in the lateral direction and disintegrating to a limited extent into small droplets.

Region C: In this case flooding is initiated at the liquid *inlet*, where a local disturbance tends to grow and block the tube. Consequently, this region is clearly observed at relatively high liquid input rates in the smaller diameter tubes employed here. Fig. 6 includes a sequence of pictures showing incipient flooding just below the liquid inlet. For the larger diameter tubes, the appearance of this region may require liquid input rates higher than those employed here.

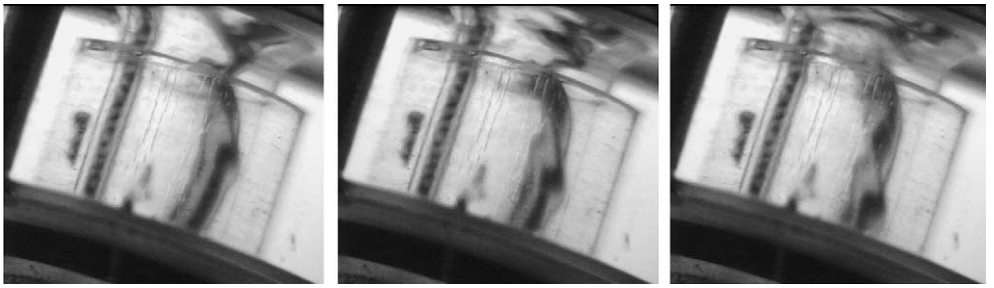

Fig. 6. A sequence of pictures showing incipient flooding just below the liquid inlet in Region C (i.d. = 7 mm, $Re_{LS} = 500$).

4. Free-flowing liquid layer thickness

Visual observations suggest that, almost up to the critical gas flooding velocity, small amplitude waves exist on the liquid surface and the mean liquid layer thickness may not differ significantly from that of the free-flowing layer in the absence of gas flow. For this reason, it was considered necessary to determine the free-flowing liquid layer thickness as a function of the liquid flow rate by carrying out experiments in the set-up of Fig. 1. Using the experimental procedures described in a previous section, the free-flowing liquid thickness was measured for two tube diameters (namely 7 and 9 mm) and two inclination angles (i.e. 30° and 60° from horizontal). Kerosene was selected for these measurements and observations, because its lower surface tension favors wave formation.

In the absence of gas flow and for the liquid flow rates employed the film surface appears to be smooth and undisturbed. Thus, considering a flat and smooth interface, the thickness of a laminar free-flowing layer may be also estimated by an approximate solution to the respective problem, which is outlined in the Appendix. For given liquid flow rate, tube diameter, inclination angle as well as liquid density and viscosity, the thickness of the free-flowing liquid layer at the tube bottom can be obtained from Eqs. (A.1) and (A.8). It will be noted that, for very small angles of inclination with respect to the vertical, Butterworth (1967) has obtained an analytical solution not applicable here.

The results of measurements and computations are presented in Fig. 7, where h is the liquid layer thickness on the vertical symmetry plane. There is fair agreement between measured values and predictions based on Eqs. (A.1) and (A.8). The greatest discrepancy is noted for $\varphi = 30°$ at relatively high Re_{LS}, where the analytical expression predicts smaller thickness, h, compared to measurements. However, the generally satisfactory agreement between measured and predicted layer thickness, h, suggests that one may employ the convenient analytical expressions (Eqs. (A.1)–(A.8)) to estimate the thickness h as well as other essential liquid layer parameters (i.e. mean real velocity, hydraulic diameter) for further data interpretation and possible correlation.

At this point, it is also of interest to estimate the liquid layer thickness near flooding by employing usual force balances on the gas and liquid phase under stratified counter-current flow with a flat interface. Considering that the pressure drop is equal in both phases, one obtains

$$\tau_G \frac{S_G}{A_G} + \tau_L \frac{S_L}{A_L} + \tau_i S_i \left(\frac{1}{A_G} + \frac{1}{A_L} \right) - (\rho_L - \rho_G) g \sin \varphi = 0 \tag{4}$$

where τ_G, τ_L, τ_i are the gas/wall, the liquid/wall and the gas/liquid interfacial shear stress, respectively; S_G, S_L are the parts of the circumference in contact with gas and liquid; S_i is the gas/liquid interface length on the tube cross-section, and A_G, A_L are the cross-sectional areas occupied by the gas and liquid phase, respectively.

The iterative approach (and relevant flow parameters) outlined by Barnea et al. (1986) is employed here to compute the thickness, h, using as basic input quantity the measured critical gas flow rate corresponding to a set of conditions (liquid flow rate, tube i.d., tube inclination angle, φ, and fluid physical properties). Fig. 8 shows a comparison of liquid layer thickness, h, obtained from Eqs. (A.1) and (A.8) as well as through the force balance method. It is interesting that the difference between the values calculated by the two methods does not exceed 10%, with the force balance method providing systematically smaller predictions. This fair agreement offers extra

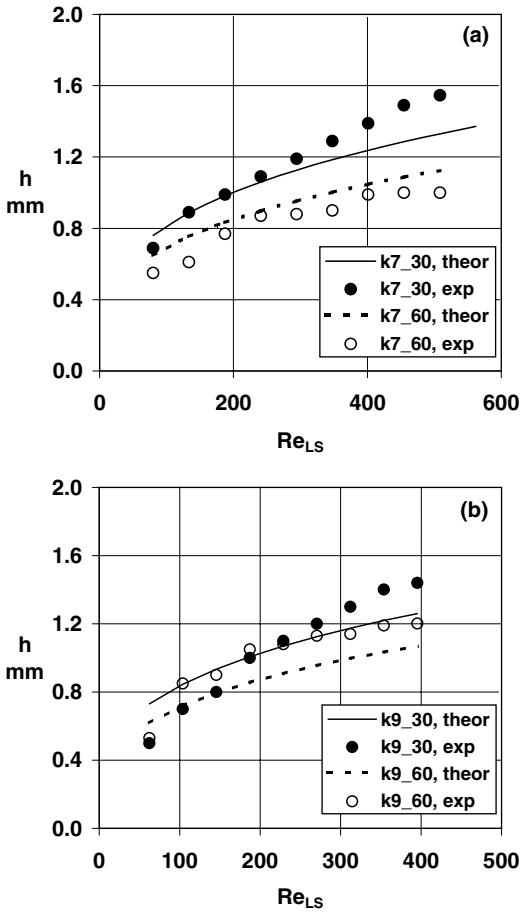

Fig. 7. Comparison of measured free-flowing liquid layer thickness, h, with theoretical predictions (Eqs. (A.1) and (A.8)) for two inclination angles: (a) i.d. = 7 mm and (b) i.d. = 9 mm.

support for employing the simple free-flowing layer expression (Eqs. (A.3)–(A.8)) to estimate the thickness, h, and other relevant parameters, useful for correlating data.

5. Discussion of results

There is experimental evidence from previous works that the critical flooding velocity tends to decrease with increasing liquid viscosity (e.g. Clift et al., 1966) and decreasing surface tension (e.g. Zapke and Kroeger, 2000b). The same trends are displayed by the results of the present study where a general observation is that the gas Reynolds number corresponding to incipient flooding is always lower in the case of kerosene, which has a higher viscosity and a lower surface tension compared to water (Table 1).

In Region A, at a fixed angle of inclination $\varphi < 90°$, the nearly linear increase of the critical gas Reynolds number, Re_{GS}, with increasing liquid Reynolds number, Re_{LS}, observed under the

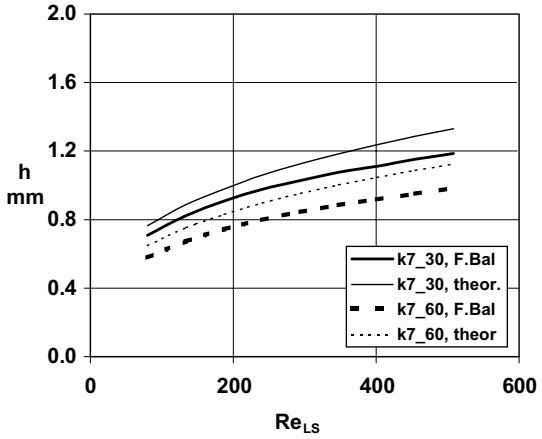

Fig. 8. Comparison of liquid layer thickness, h, obtained from Eqs. (A.1) and (A.8) (marked "theor.") and through the force balance method (marked "F.Bal.") for kerosene and two inclination angles.

conditions of the present experiments (Fig. 3), has not been reported in the literature before. There is no obvious explanation for this trend. One may hypothesize that, in this range of small liquid rates with high tube curvature (i.e. in small i.d. tubes) lateral liquid spreading readily takes place, effectively reducing the amplitude of waves especially near the liquid exit where the onset of liquid flow reversal is observed. Thus, in this small-Re_{LS} range, considering that the wave shape does not change significantly with increasing liquid rate, an increased gas velocity would be required to generate high enough drag on the waves to counterbalance gravitational forces and to reverse wave motion. The fairly symmetrical "ring"-type waves moving upwards tend to support this argument applying to Region A. Increasing the liquid rate above a certain value (Region B), the thicker and faster moving layer at the tube bottom would tend to favor the formation of 3-D waves (with reduced lateral spreading), which would grow and reverse their flow direction but at progressively smaller gas velocities. Visual observations suggest that this picture is typical of incipient flow reversal in Region B. The tendency for Region A to vanish with increasing tube i.d. and the appearance of 3-D waves moving upwards lends support to the above explanation.

Attention will be focused here on Region B, which is encountered in all data sets, and it is the most extensive one. From the visual observations and the careful inspection of the experimental results it can be concluded that the gas velocity necessary to cause incipient flooding is the outcome of the interaction of several parameters, the most important of which are as follows:

- The physical *properties* of the liquid phase, mainly the surface tension and the viscosity; as pointed out above this dependence is represented by an expression of the form $U_G \propto \frac{\sigma^n}{\mu^m}$, where the exponents m, n are positive numbers.
- The *liquid layer velocity*; it is observed that the gas flooding velocity is roughly inversely proportional to the liquid velocity ($U_G \propto U_L^{-1}$).
- The tube *diameter*; critical flooding velocity tends to increase with increasing tube i.d. ($U_G \propto D^n$), although this trend is not very pronounced.
- The tube *inclination angle*; an increasing critical gas velocity is observed with decreasing angle of inclination in the range tested (i.e. 30–60°).

An attempt is made to develop a correlation to take into account the trends outlined above. The effect of liquid layer velocity, liquid layer thickness as well as liquid properties may be included by defining an appropriate liquid Froude number:

$$Fr_{\mathrm{LH}} = \frac{\langle U_{\mathrm{L}} \rangle^2}{D_{\mathrm{LH}} g \sin \varphi}$$

where $\langle U_{\mathrm{L}} \rangle = \frac{Q_{\mathrm{L}}}{A_{\mathrm{L}}}$ is the mean liquid layer velocity, D_{LH} is the hydraulic diameter of the liquid phase "conduit" and φ is the tube inclination with respect to horizontal position. The liquid layer cross-section, A_{L}, can be calculated from the tube diameter and the mean liquid layer thickness, h; the latter can be predicted using Eqs. (A.1) and (A.8). Similarly, the effect of gas velocity, gas cross-section and gas kinematic viscosity can be incorporated in the gas Reynolds number defined as

$$Re_{\mathrm{GH}} = \frac{\langle U_{\mathrm{G}} \rangle D_{\mathrm{GH}}}{\nu_{\mathrm{G}}}$$

where $\langle U_{\mathrm{G}} \rangle = \frac{Q_{\mathrm{G}}}{A_{\mathrm{G}}}$ is the mean gas velocity and D_{GH} is the hydraulic diameter of the gas phase conduit. It is noted that data with different gases would help elucidate gas Reynolds number effects.

Finally, the effect of liquid properties is taken into account by using the Kapitsa number defined as:

$$Ka = \frac{\sigma_{\mathrm{L}}}{(\nu_{\mathrm{L}} g \sin \varphi)^{1/3} \mu_{\mathrm{L}}}$$

The use of the Kapitsa number is also supported by the theoretical analysis carried out by Cetinbudaklar and Jameson (1969), which shows that for low liquid viscosity the critical gas flooding velocity tends to increase with the Kapitsa number to a power near 0.5 (Fig. 6 of their paper). These authors apply small amplitude stability analysis (in a two-dimensional geometry) to predict critical gas velocity required to cause unstable waves. Direct comparison of their results with those of the present three-dimensional case cannot be made.

In Fig. 9 the quantity $Re_{\mathrm{GH}}/Ka^{0.4}$ at flooding point is plotted against the corresponding liquid Froude number, Fr_{LH}. It is evident that the data points (excluding those of Region A) tend to fall roughly along a line of the following form:

$$\frac{Re_{\mathrm{GH}}}{Ka^{0.4}} = a Fr_{\mathrm{LH}}^{-0.5}.$$

This correlation appears to provide first estimates of (possibly a maximum) critical flooding velocity for relatively small viscosity fluids and small i.d. tubes. It is worth noting that this correlation is consistent essentially with all major dependencies of the critical gas velocity outlined above.

Fig. 10a includes data obtained with water by Zapke and Kroeger (2000a), by Wongwises (1998) as well as in this study, at an inclination angle 60°. The closest available data by Celata et al. (1992) and Barnea et al. (1986) are also plotted there. The data by Celata et al. and Zapke and

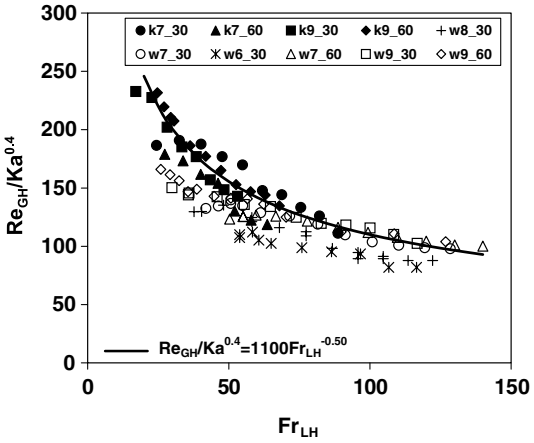

Fig. 9. The quantity $Re_{GH}/Ka^{0.4}$ at flooding point plotted against the corresponding liquid Froude number.

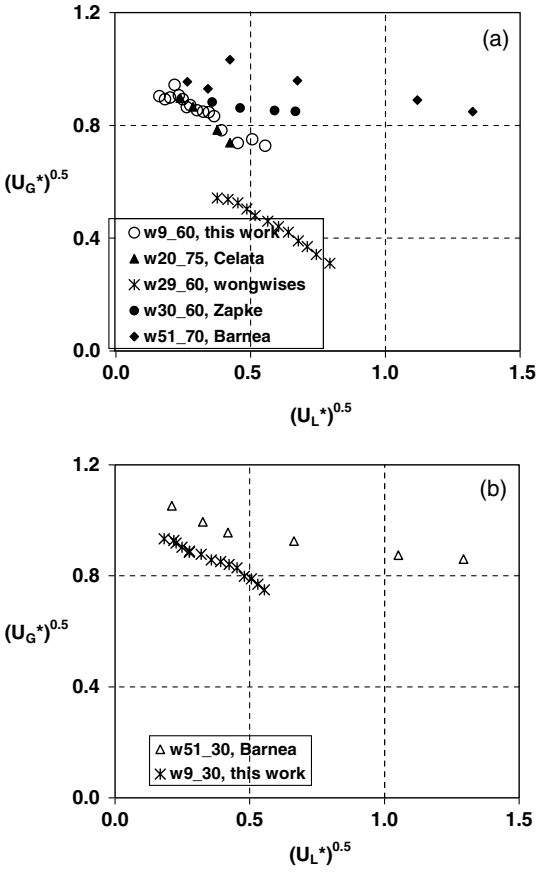

Fig. 10. Comparison in a Wallis-type plot of representative data from the literature with typical data from this study; (a) experimental data at $\varphi = 60°$, data by Celata et al. (1992) at $\varphi = 75°$, by Barnea et al. (1986) at $\varphi = 70°$, by Wongwises (1998) at $\varphi = 60°$ and by Zapke and Kroeger (2000a) at $\varphi = 60°$; (b) $\varphi = 30°$.

Kroeger are in general agreement with the present measurements; the sharp edged gas entry in the former case, as opposed to smooth tapered entry in the latter, may be responsible for this difference. The data by Wongwises, although apparently obtained under similar conditions as those of Zapke and Kroeger, display quite small critical flooding velocities. The data of Barnea et al. for 60° and 30° angle, compared with the present data in Fig. 10a and b respectively, tend to be significantly higher. Whether this is due to the much larger tube diameter (51 mm versus 9 mm), and possibly to a different mechanism for incipient flooding, or due to differences of the experimental set-up and procedure, it is difficult to ascertain. It will also be noted that the correlation (Eq. (1)) proposed by Zapke and Kroeger (1996) does not perform well with the present data.

The critical flooding velocities obtained by Mouza et al. (2002) for *vertical tubes* are significantly smaller than the ones reported here for inclined tubes, throughout the range of flow rates tested. Moreover, in the range of angles tested, the present data (e.g. Fig. 3) show that, for a fixed liquid input rate, the critical gas flooding velocity tends to decrease with increasing angle of inclination. This observation does not seem to be in accord with the reported findings by Barnea et al. (1986) in a 51 mm i.d. tube, summarized in Introduction.

6. Concluding remarks

At small Re_{LS} (with the smallest i.d. tubes tested), the critical gas velocity for incipient flooding, U_{GS}, tends to *increase* almost linearly with Re_{LS}, a trend not reported in the literature before. This might be due to lateral spreading of liquid (near the exit) facilitated by the large curvature of the tube (small i.d.). At intermediate Re_{LS} (Region B) the flooding velocity, U_{GS}, tends to decrease with increasing liquid input rate, as observed with relatively large i.d. tubes in the literature. Growth of 3-D waves (possibly due to instability) near the liquid exit and reversal of their flow direction is the mechanism for incipient flooding in this region. At relatively high Re_{LS} (Region C) the flooding velocity, U_{GS}, tends to reach a constant value i.e. to be independent of liquid input rate. Growth of disturbances at liquid *inlet* and flow reversal appears to be responsible for this trend.

With the present experimental set-up, and the rather small i.d. tubes tested, the free-flowing liquid layer (in the absence of gas) exhibits a smooth surface with only shallow waves (of long wavelength) appearing at the higher Re_{LS} investigated. An approximate analytical solution for the laminar free-flowing layer is in fair agreement with measurements of the liquid layer thickness in the absence of gas flow. This approximate solution is convenient for estimating liquid layer thickness, thus facilitating interpretation and correlation of the flooding data. It is also interesting that a mean force balance method, applied at gas and liquid rates corresponding to flooding, leads to an estimate of liquid layer thickness in substantial agreement with the approximate analytical solution. This may not be surprising because it has been already reported in the literature (e.g. Dukler et al., 1984) that the mean liquid layer thickness does not change significantly, even close to flooding conditions.

The presently reported data have been obtained with one gas and two different liquids. Additional data are certainly needed, with other liquids and gases (covering a broader range of physical properties), in order to elucidate the effects of liquid and gas properties and to assess the significance of dimensionless numbers (notably of gas Reynolds number and of Kapitsa number) employed for generalized correlations. Work along these lines is in progress.

Acknowledgement

Financial support by the European Commission under contract JOE3-CT97-0062 is gratefully acknowledged.

Appendix A. Laminar flow of a thin liquid layer on an inclined tube

The flow geometry is defined in Fig. 11. The following assumptions are made

- Flat free surface, with a maximum free-flowing layer thickness given by

$$h = R(1 - \cos \Theta) \tag{A.1}$$

- Unidirectional laminar flow.
- A layer sufficiently thin so that the condition $\frac{du_z}{dr} = 0$ holds at the free surface.

The simplified equation of motion is

$$\mu\left[\frac{1}{r}\frac{\partial}{\partial r}\left(r\frac{\partial u_z}{\partial r}\right)\right] + \rho g_z = 0 \tag{A.2}$$

where u_z and g_z are the velocity and gravity components parallel to the tube axis, respectively. For an angle of inclination φ, with respect to the horizontal plane $g_z = g \sin \varphi$.

Integrating Eq. (A.2) with the boundary conditions

$$u_z = 0 \text{ at } r = R \quad \text{and} \quad \frac{du_z}{dr} = 0 \text{ at } r = R\frac{\cos \Theta}{\cos \vartheta}$$

the various flow parameters are obtained as follows:

$$u_z = \frac{\rho g_z R^2}{4\mu}\left[1 - \left(\frac{r}{R}\right)^2 + 2\frac{\cos^2 \Theta}{\cos^2 \vartheta}\ln\left(\frac{r}{R}\right)\right] \tag{A.3}$$

at the free surface where $r = R\frac{\cos \Theta}{\cos \vartheta}$

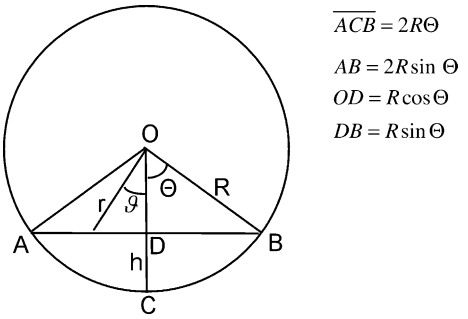

Fig. 11. The main parameters for the definition of the flowing layer thickness.

$$(u_z)_i = \frac{\rho g_z R^2}{4\mu}\left[1 - \frac{\cos^2\Theta}{\cos^2\vartheta} + 2\frac{\cos^2\Theta}{\cos^2\vartheta}\ln\left(\frac{\cos\Theta}{\cos\vartheta}\right)\right] \tag{A.4}$$

$$(u_z)_{\max}\big|_{\vartheta=0} = \frac{\rho g_z R^2}{4\mu}\left[\sin^2\Theta + 2\cos^2\Theta\ln(\cos\Theta)\right] \tag{A.5}$$

$$\tau_{rz} = \frac{\rho g_z}{2}r - \frac{\rho g_z}{2}\left(R\frac{\cos\Theta}{\cos\vartheta}\right)^2\frac{1}{r} \tag{A.6}$$

$$\tau_w = \tau_{rz}\big|_{r=R} = \frac{\rho g_z}{2}R\left(1 - \frac{\cos^2\Theta}{\cos^2\vartheta}\right) \tag{A.7}$$

$$Q = \frac{\rho g_z R^4}{6\mu}\left[\frac{\sin 4\Theta}{4} - \Theta\cos 2\Theta - \frac{\Theta\cos 4\Theta}{4} - \frac{\sin 2\Theta}{9}\right] \tag{A.8}$$

For a given liquid flow rate, Q, and tube geometry, the liquid layer thickness, h, is given implicitly by Eqs. (A.1) and (A.8)

References

Bankoff, S.G., Lee, S.C., 1986. A critical review of the flooding literature. In: Hewitt, G.F., Delhaye, J.M., Zuber, N. (Eds.), Multiphase Science and Technology, vol. 2. Hemisphere Corp, NY (Chapter 2).

Barnea, D., Ben Yosef, N., Taitel, Y., 1986. Flooding in inclined pipes—effect of entrance section. Can. J. Chem. Eng. 64, 177–184.

Butterworth, D., 1967. The laminar flow of liquid down the outside of a rod which is at a small angle from the vertical. Chem. Eng. Sci. 22, 911–924.

Celata, G.P., Cumo, M., Setaro, T., 1992. Flooding in inclined pipes with obstructions. Exp. Thermal Fluid Sci. 5, 18–25.

Cetinbudaklar, A.G., Jameson, G.J., 1969. The mechanism of flooding in vertical countercurrent two-phase flow. Chem. Eng. Sci. 24, 1669–1680.

Clift, R., Pritchard, C.L., Nederman, R.M., 1966. The effect of viscosity on the flooding conditions in wetted wall columns. Chem. Eng. Sci. 21, 87–95.

Dukler, A.E., Smith, L., Chopra, A., 1984. Flooding and upward film flow in tubes—I. Int. J. Multiphase Flow 10, 585–597.

Govan, A.H., Hewitt, G.F., Richter, H.J., Scott, A., 1991. Flooding and churn flow in vertical pipes. Int. J. Multiphase Flow 17, 27–44.

Hewitt, G.F., 1977. Influence of end conditions, tube inclination and fluid physical properties on flooding in gas–liquid flow. UKAEA Report HTFS-RS222.

Hewitt, G.F., 1995. In search of two-phase flow, Lecture. In: 30th US National Heat Transfer Conference, Portland, Oregon.

Mouza, A.A., Paras, S.V., Karabelas, A.J., 2002. The influence of small tube diameter on falling film and flooding phenomena. Int. J. Multiphase Flow 28, 1311–1331.

Pierson, F.W., Whitaker, S., 1977. Some theoretical and experimental observations of the wave structure of falling liquid films. Ind. Eng. Chem. Fund. 16, 401–408.

Wallis, G.B., 1969. One-dimensional Two-phase Flow. McGraw-Hill, New York.

Wongwises, S., 1998. Effect of inclination angles and upper end conditions on the countercurrent flow limitation in straight circular pipes. Int. Commun. Heat Mass Transfer 25, 117–125.

Zapke, A., Kroeger, D.G., 1996. The influence of fluid properties and inlet geometry on flooding in vertical and inclined tubes. Int. J. Multiphase Flow 22, 461–472.

Zapke, A., Kroeger, D.G., 2000a. Counter-current gas–liquid flow in inclined and vertical ducts—I: flow patterns, pressure drop characteristics and flooding. Int. J. Multiphase Flow 26, 1439–1455.

Zapke, A., Kroeger, D.G., 2000b. Counter-current gas–liquid flow in inclined and vertical ducts—II: the validity of the Froude–Ohnesorge number correlation for flooding. Int. J. Multiphase Flow 26, 1457–1468.